ACS Energy LETTERS

Cite This: ACS Energy Lett. 2019, 4, 1225−1230

http://pubs.acs.org/journal/aelccp

LETTER

Controlled Steric Hindrance Enables Efficient Ligand Exchange for Stable, Infrared-Bandgap Quantum Dot Inks

Mengxia Liu,[‡,¶] Fanglin Che,[‡,¶] Bin Sun,[‡] Oleksandr Voznyy,[‡] Andrew Proppe,[‡,†] Rahim Munir,[§,∥] Mingyang Wei,[‡] Rafael Quintero-Bermudez,[‡] Lilei Hu,[⊥] Sjoerd Hoogland,[‡] Andreas Mandelis,[‡,⊥] Aram Amassian,[§] Shana O. Kelley,[†,#] F. Pelayo García de Arquer,[‡] and Edward H. Sargent*[,‡]

[‡]Department of Electrical and Computer Engineering, University of Toronto, 10 King's College Road, Toronto, Ontario M5S 3G4, Canada

[†]Department of Chemistry, University of Toronto, 80 St. George Street, Toronto, Ontario M5S 3H6, Canada

[§]King Abdullah University of Science and Technology (KAUST), KAUST Solar Center (KSC), Physical Sciences and Engineering Division, 4700 KAUST, Thuwal 23955-6900, Saudi Arabia

[∥]Helmholtz-Zentrum Berlin für Materialien und Energie, Kekuléstrasse 5, Berlin 12489, Germany

[⊥]Center for Advanced Diffusion-Wave and Photoacoustic Technologies (CADIPT), Department of Mechanical and Industrial Engineering, University of Toronto, Toronto, Ontario M5S 3G8, Canada

[#]Department of Pharmaceutical Sciences, Leslie Dan Faculty of Pharmacy, University of Toronto, Toronto, Ontario M5S 3M2, Canada

Supporting Information

ABSTRACT: **Colloidal quantum dots (CQDs), which benefit from a size-tuned bandgap, are a solution-processed material for infrared energy harvesting. This characteristic enables the fabrication of solar cells that form tandem devices with silicon. Unfortunately, in the case of CQDs having diameters sufficiently large (>4 nm) so that the nanoparticles absorb light well beyond silicon's bandgap, conventional ligand exchanges fail. Here we report a strategy wherein short-chain carboxylates, used as a steric hindrance controller, facilitate the ligand exchange process on small-bandgap CQDs. We demonstrate that the net energy barrier to replace original capping ligands with lead halide anions is decreased when short carboxylates are involved. The approach produces more complete ligand exchange that enables improved packing density and monodispersity. This contributes to a 2-fold reduction in the trap state density compared to the best previously reported exchange. We demonstrate solar cells that achieve a record infrared photon-to-electron conversion efficiency at the excitonic peak.**

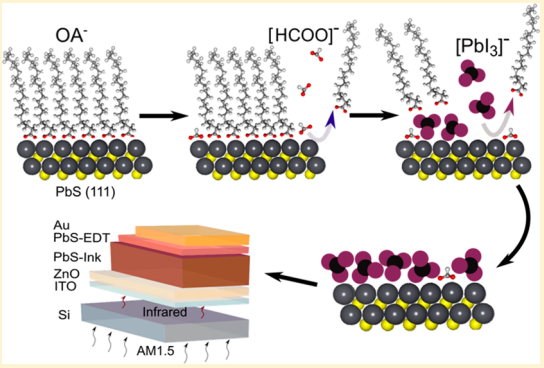

Colloidal quantum dots (CQDs) are emerging solution-processed materials that have generated interest for their applications in optoelectronic devices.[1−6] Single-junction metal chalcogenide CQD solar cells[6−8] have recently achieved certified power conversion efficiencies (PCEs) of 12%.[9]

Spectral tunability[10,11] is among the advantages of CQD solar technology: the absorption edge can be readily tuned across the solar spectrum by adjusting the size of CQDs at the time of synthesis.[12] This offers avenues to tandem and multijunction solar cells, where CQDs can be used as back cell materials to harvest infrared light transmitted through other photovoltaic (PV) materials such as silicon and perovskites.[13−15]

Silicon-based solar cells account for over 90% of global solar energy production.[16,17] They transmit over 15% of the sun's power that lies beyond their 1100 nm absorption edge. Up to 6 absolute power points can be added atop the PCE of the best silicon cells when sunlight at wavelengths beyond 1100 nm is harvested.[13]

Received: February 19, 2019
Accepted: April 30, 2019
Published: April 30, 2019

DOI: 10.1021/acsenergylett.9b00388
ACS Energy Lett. 2019, 4, 1225−1230

Recent studies have reported printable CQD inks that provide infrared light harvesting.[14,15] Intensive efforts on device engineering have improved the infrared PCE to greater than 1%.[15] This approach relies on a mixture of multibandgap CQDs to tailor the density of states. The solution-phase ligand exchange method was applied to CQDs of each size to avoid disruptive place exchanges in the solid state;[6] however, this functioned poorly when applied to CQDs having a longer-wavelength infrared bandgap. Previously reported ligand exchange methods provide insufficient chemical reactivity to replace original capping ligands from large-diameter CQDs, a consequence of the distinct and varied facets exposed on the larger dots.[15,18,19] The strong steric hindrance of the original capping ligands prevented the diffusion of the lead halide, leading to a large energy barrier to ligand exchange. Consequently, an appreciable fraction of the original ligands remains on the CQD surface, resulting in poor carrier transport and increased heterogeneity. Precursor solutions with strong chemical reactivity easily etch CQD surfaces, making the CQD dispersion less stable.

We sought a new means to promote the desired ligand exchange while preserving colloidal stability. Herein we find that a small amount of short-chain carboxylates (formate, acetate, and propionate) facilitate the exchange process through control over steric hindrance. We demonstrate a more complete removal of original ligands when applying shorter-chain carboxylates together with halide ligands.[20,21] The presence of short-chain carboxylates shifts the oleates from their optimal binding geometries because of steric hindrance and provides a channel for increased access of halides to CQD surfaces. This significantly reduces the energy barrier to lead halide exchange and increases the resultant halide coverage on the surface. It allows thereby for improved carrier transport while at the same time enhancing spatial homogeneity. This allows us to fabricate solar cell devices with single-sized infrared-bandgap quantum dots and achieve record external quantum efficiency (EQE) at the exciton peak. This contributes to a filtered power conversion efficiency (PCE) of 0.96 power points atop the PCE of a front Si cell even though the IR cells utilize only a portion of the spectrum between 1100 and 1350 nm.

The ligand exchange process in the presence of formate species is depicted in Figure 1a. To gain an improved atomistic picture of this process, we employed density functional theory (DFT) using the Vienna Ab Initio Simulation Package (VASP) code (Figure 1b and Supporting Information section 3).[22,23]

Prior to ligand exchange, CQDs are capped by OA^- with a surface coverage of 80%.[24] Higher coverage is not possible because of steric hindrance. Nevertheless, when CQDs are mixed vigorously with a precursor solution containing lead halide and ammonium formate in *N*,*N*-dimethylformamide (DMF), formate species are able to diffuse between oleic acid ligands and adsorb onto the OA-free sites on a PbS(111) facet, with a favorable binding energy of −0.4 eV/$HCOO^-$, whereas the adsorption of more oleates is already unfavorable (Figure S1). This effect arises from formate's small spatial footprint and strong adsorption energy (Figures S2 and S3). After the formate-assisted ligand exchange, CQDs were well-dispersed in DMF after phase separation. For the exchange lacking of small carboxylate molecules, however, the phase separation took a longer time and CQDs aggregated in DMF solution.

DFT calculations indicate that adsorbed formate molecules decrease the reaction energy associated with OA^- removal and

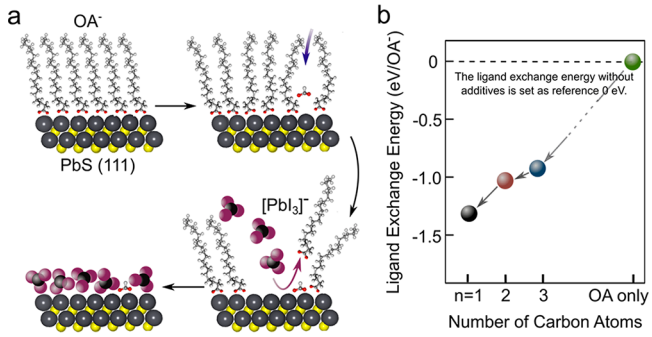

Figure 1. CQD ligand exchange assisted by the use of short-chain carboxylates. (a) Schematic depicting formate-assisted ligand exchange on PbS(111) facets. (b) DFT calculations of the ligand exchange energy improvement compared to the OA-only case ($\Delta H_{rxn}'$). The reaction energy of the ligand exchange without short-chain carboxylates is set as reference 0 eV (green dot). A more negative energy value corresponds to a more favorable reaction. The data show that the ligand exchange is favored when shorter carboxylate additives ($RCOO^-$, R = H, CH_3, C_2H_5) are used. Details of the DFT methodology are included in Supporting Information section 3.

PbI_3^- adsorption by as much as 1.3 eV/OA^-, promoting the ligand exchange to a significant degree (Figure 1b). The energy favorability is due to the increased ligand packing density and, thus, enhanced steric repulsion between OA^- ligands, which forces them to rearrange and adopt less favorable binding geometries.[25,26] Other small carboxylates also facilitate the ligand exchange process, with the benefit decreasing as the carbon chains become longer.

In light of these findings, we examined the surfaces of exchanged CQDs using proton nuclear magnetic resonance (^{1}H NMR) spectroscopy.[26] All exchanged CQDs are dispersed in deuterated DMF with the same concentration. Ferrocene is added as an internal standard for quantitative comparison.

The ^{1}H NMR spectrum of formate-assisted exchanged CQDs in Figure 2a shows a distinct aldehyde peak at 10.04 ppm. Comparison among the spectra of functionalized CQDs (Figures 2a, S4, and S5) versus free ligand (Figures S6 and S7) indicates that formate binds to the CQD surface following solution exchange. This is evidenced by the observed spectral broadening attributable to slower tumbling of the molecules[27−29] in solution and an inhomogeneous magnetic CQD surface.[27,30] A small peak at 5.52 ppm represents the double bond from oleic acid left over on the CQD surface.

We then studied surface coverage when different carboxylates are used for ligand exchange. The determination takes into account the CQD concentration, ferrocene concentration, and ^{1}H NMR signal ratios (Supporting Information section 4). The result reveals an average of 25 formate molecules adsorbed per dot in the formate-exchanged sample (~5% surface coverage). The alkyl hydrogen at 1.96 ppm can be detected for the acetate-exchanged sample (Figure S4); however, the peak is too small to be accurately quantified. The alkyl hydrogen peaks from propionate overlap with the solvent peak and are close to the detection limit.

We then calculated the total organic anions and lead halide ligands binding to quantum dot surfaces with the aid of data obtained using X-ray photoelectron spectroscopy (XPS). The calculation results are summarized in Table 1. The ratio of carbon to lead decreases from 16.5 to 0.4 following formate-assisted ligand exchange. Consistent with DFT results, less

DOI: 10.1021/acsenergylett.9b00388
ACS Energy Lett. 2019, 4, 1225−1230

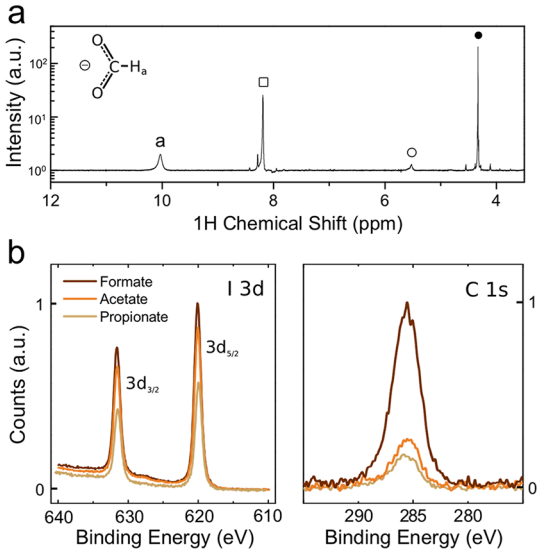

Figure 2. (a) ^{1}H NMR spectra of formate-assisted exchanged PbS CQD surface. The aldehyde signal from bound formate is labeled a. The double bond from oleic acid residue is marked using a black circle (○). The black dot (●) represents the peak from ferrocene, the internal standard for quantitative comparison. The peak from trace nondeuterated solvent is marked using a black square (□). (b) XPS measurements showcase the halide coverage and OA^{-} residues after ligand exchange.

Table 1. Summary of Ligand Coverage of PbS CQD Surfaces

	NMR	XPS	
surface capping ligands	$RCOO^{-}$ per dot (R = H, CH_3, C_2H_5)	carbon-to-Pb ratio	halogen (I and Br)-to-Pb ratio
formate-exchanged	25	0.4	0.9
acetate-exchanged	too small to quantify	0.6	0.7
propionate-exchanged		1.8	0.6
unexchanged		16.5	0

carbon is detected when shorter-chain carboxylates are used, indicating a more complete removal of OA^{-}. The ratio of halogen (iodine and bromine) to lead follows the opposite trend, showing a ratio of 0.9 for the formate-assisted exchange, which is higher than the values of 0.7 and 0.6 for acetate and propionate, respectively (Figures 2b and S8).

These findings, taken together, show that the formate sample maintains the highest carboxylate coverage, a fact that we correlate with the strong binding energy of formate obtained using DFT. This leads to the highest halogen-to-Pb ratio in the final dots, again traceable to the lowered exchange reaction energy. The formate sample also has the lowest amount of unbound carbon, a fact that we projected would facilitate improved carrier transport.

We then investigated the effect of ligand exchange on packing and energetic homogeneity. Grazing-incidence small-angle X-ray scattering (GISAXS) is used to determine the average center-to-center spacing of nanoparticles as well as their packing uniformity. A hexagonal diffraction pattern is observed for exchanged CQDs, showing an orientational in-plane ordering (Figures 3a and S9, Table S1). It is also found

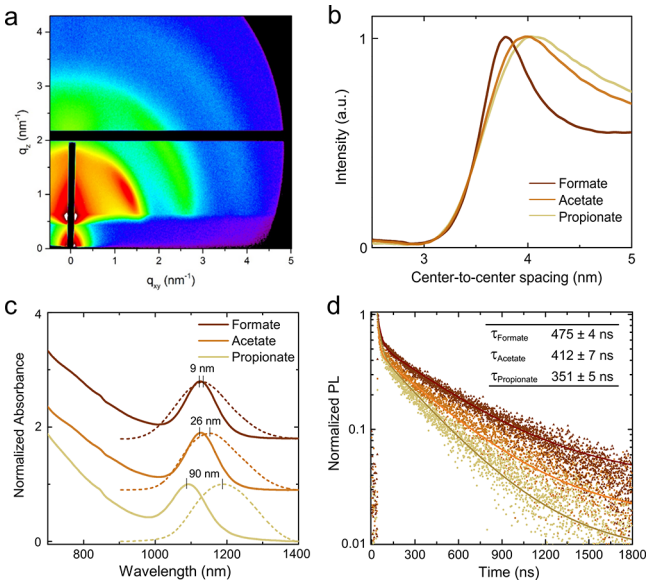

Figure 3. (a) Two-dimensional GISAXS pattern of the formate-exchanged film. Blue represents low intensity, and red represents high intensity. The vertical black line on the left corner is the beam stop, and the horizontal one is because of the Pilatus 200k detector. (b) Azimuthally integrated GISAXS intensities showing the distribution of center-to-center spacing of nanoparticles for different films. Shorter-chain carboxylates lead to closer spacing and better monodispersity. (c) Stokes shifts of exchanged solutions. The smallest Stokes shift for the formate sample indicates the sharpest bandtail and a minimum of energy transfer. (d) Photocarrier lifetimes in exchanged solutions.

that the center-to-center spacing decreases from 4.1 nm for propionate-exchanged films to 3.8 nm for the case of formate. The distribution of particle separation length also becomes narrower following the same trend (Figure 3b). No significant change in CQD morphology is observed in TEM images (Figure S10). This suggests that by reducing the OA bonding strength, overtreatment is successfully avoided, leading to an improved energetic homogeneity.

The energy transfer between CQDs with different bandgaps in a polydispersed ensemble was reported to contribute to excess Stokes shift[31] (the energy difference between emission and absorption peaks).[32] As a result, the Stokes shift in solution reflects CQD size polydispersity and the degree of aggregation.

To explicitly test the energy transfer between CQDs in exchanged solutions, we tested the Stokes shift for three samples using dilute solutions (0.1 mg/mL) to avoid reabsorption and slow down the energy transfer.[33] The smallest Stokes shift (9 nm) is observed for the formate-exchanged sample, indicating the minimal degree of aggregation and energy transfer (Figure 3c) due to improved surface coverage with ligands. This indicates that improved surface coverage results in reduced CQD aggregation. Formate-exchanged samples also show the longest photoluminescence lifetime of 470 ns, a fact we associated with improved surface passivation (Figure 3d and Table S2).

Through field-effect transistor (FET) measurements, we further investigated the electronic landscape for charge carriers in the various thin films. We fabricated FET devices following a reported bottom-gate top-contact configuration (Figure S11). Titanium and zirconium oxide are deposited on a glass

DOI: 10.1021/acsenergylett.9b00388
ACS Energy Lett. 2019, 4, 1225−1230

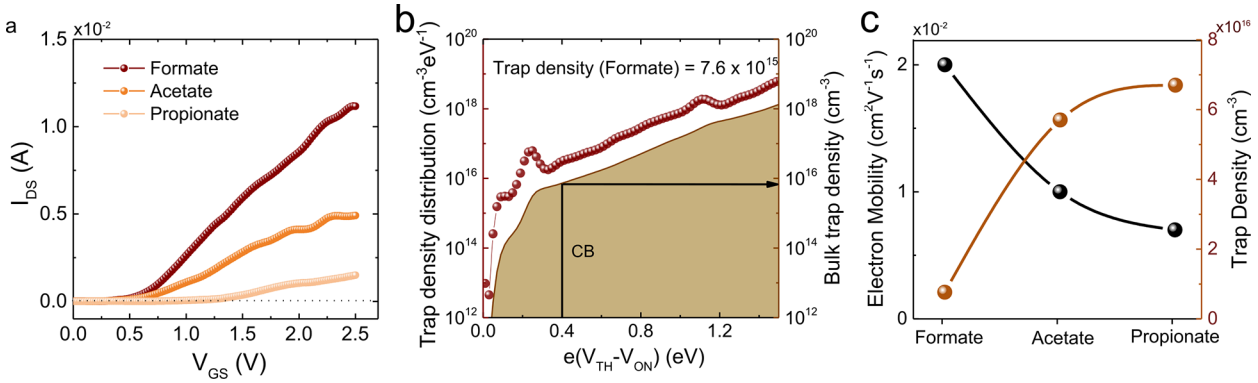

Figure 4. FET study on mobilities and trap densities of exchanged CQD solids. (a) Transfer characteristics of exchanged CQD films. (b) Trap state densities of the formate sample. (c) Summary of trap density and electron mobility of various samples. The formate-assisted exchanged film has an electron mobility of 0.02 $cm^2\ V^{-1}\ s^{-1}$, twice as high as that of acetate counterparts, and a significantly low trap density of $8 \times 10^{15}\ cm^{-3}$.

substrate as gate and dielectric layers, respectively. This is followed by spin-coating a CQD film with a thickness of 150 nm, completed by a gold top contact.

Linear transfer characteristics were demonstrated at a drain voltage of 100 mV (Figure 4a). The carrier mobility is calculated from the slope of the linear region:[34] the formate-assisted exchanged film has an electron mobility of 0.02 $cm^2\ V^{-1}\ s^{-1}$, twice as high as that of the acetate and propionate controls (Figure 4c). We ascribe the improved mobility to the complete removal of OA and also improved monodispersity.

The density of bandtail states can be estimated from the subthreshold region of transfer characteristics.[35] As the gate bias varies from turn-on voltage to threshold voltage, the drain current shows an exponential increase, and this corresponds to a gradual filling of bandtail states, leading to improved transport.[36] It can also be used to estimate the trap state density. We obtain the bandtail state density in formate-exchanged films of $8 \times 10^{15}\ cm^{-3}$. This is significantly lower than $5 \times 10^{16}\ cm^{-3}$ for the control, indicating the reduction in bandtail states arising from the more complete ligand exchange (Figures 4b,c and S12).

We then pursued CQD photovoltaic device performance. Devices were fabricated in the architecture of Figure 5a. Underneath the CQD device, a long-pass filter was employed to emulate the filtering of AM1.5 solar irradiation using a silicon front cell.

We first fabricated CQD devices over a range of CQD sizes and found the most suitable bandgap, of around 1.05 eV, that achieved the highest filtered PCE (Figure 5b). When the bandgap is further decreased beyond this value, the slow increase in short-circuit current (J_{sc}) did not compensate for the loss in V_{oc}.

Thickness-dependence studies on CQD devices using different exchange protocols allowed us to characterize the impact of the exchange on transport lengths.[37] As the active layer thickness is increased from 250 to 360 nm, the PCE of formate-exchanged devices improves under both full solar spectrum and also the filtered (infrared) one; however for acetate and propionate ones, performance starts to decrease at lower thicknesses (Figure S13a,b). This indicates an enhanced charge carrier diffusion length for formate-exchanged CQDs compared to controls. We demonstrate as a result CQD solar cells that, by harvesting below-silicon-bandgap infrared light, augment silicon with an additional 0.96 absolute power points.

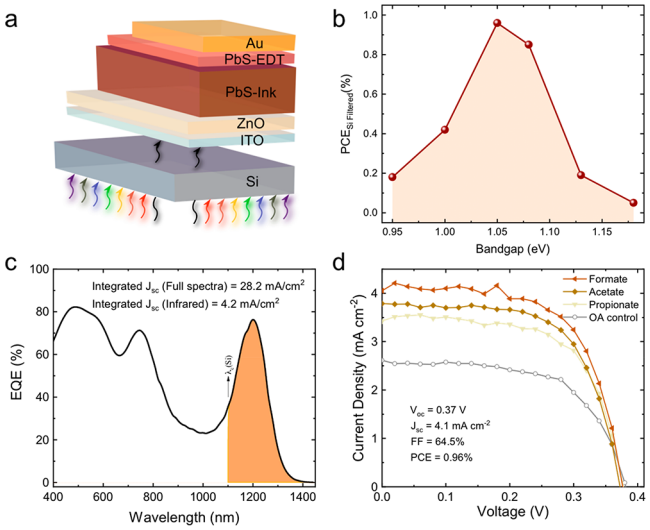

Figure 5. Experimental optoelectronic investigations of infrared CQD solar cells using filtered solar spectra through silicon. (a) Infrared device architecture. (b) Device performance of formate-exchanged CQD solids having different bandgaps. (c) EQE spectra of the champion formate-exchanged infrared device. (d) Performance of CQD devices using different exchange protocols.

The dramatic advance in performance for the optimal formate-exchanged device originates mainly from the significant improvement in the product of current density and fill factor (FF): the filtered J_{sc} reaches 4.1 mA cm^{-2} and is combined with a FF of 64% (Figure 5d and Table S3). The record devices show an EQE at exciton of 76%, reconfirming improved electron collection and reduced recombination losses (Figures 5c and S14).

The formate-assisted devices showed no degradation following 200 h of storage in air without encapsulation (Figure S15a). They also demonstrated improved thermal stability which we associate with enhanced surface passivation: the control devices start to degrade after 20 min of annealing at 100 °C, and their performance drops ∼20% after 40 min; however, the formate-assisted devices show less than 10% loss in PCE after annealing for the same duration of time (Figure S15b).

In this work, we report a strategy to facilitate a more complete ligand exchange on small-bandgap CQDs. The

DOI: 10.1021/acsenergylett.9b00388
ACS Energy Lett. 2019, 4, 1225−1230

approach employs short-chain carboxylate groups to increase ligand packing density, forcing oleates to rearrange because of steric effects—a fact that ultimately weakens their binding. We found that the use of formate promotes solution exchange to lead halide and provides halide-saturated surfaces exhibiting less OA residue. CQD solids exhibit lower bandtailing and reduced energetic disorder, contributing to a lower recombination loss and improved charge carrier mobility. These joint benefits, arising from the surface chemical control, allow us to construct thick-active-layer infrared CQD solar cells that absorb more light and generate an increased current without deteriorating V_{oc} and FF.

■ ASSOCIATED CONTENT

Supporting Information

The Supporting Information is available free of charge on the ACS Publications website at DOI: 10.1021/acsenergylett.9b00388.

Experimental details; DFT calculations; additional ^{1}H NMR, XPS, and GISAXS data; additional device performance and FET measurements (PDF)

■ AUTHOR INFORMATION

Corresponding Author

*E-mail: ted.sargent@utoronto.ca.

ORCID

Mengxia Liu: 0000-0002-1676-705X
Oleksandr Voznyy: 0000-0002-8656-5074
Rafael Quintero-Bermudez: 0000-0002-4233-395X
Shana O. Kelley: 0000-0003-3360-5359
Edward H. Sargent: 0000-0003-0396-6495

Author Contributions

¶M.L. and F.C. contributed equally.

Notes

The authors declare no competing financial interest.

■ ACKNOWLEDGMENTS

This publication is based in part on work supported by the Ontario Research Fund Research Excellence Program and by the Natural Sciences and Engineering Research Council (NSERC) of Canada. Computations were performed on the Niagara supercomputer at the SciNet HPC Consortium. SciNet is funded by: the Canada Foundation for Innovation; the Government of Ontario; Ontario Research Fund Research Excellence Program; and the University of Toronto. The authors thank E. Palmiano, L. Levina, R. Wolowiec, and D. Kopilovic for their help during the course of this study.

■ ABBREVIATIONS

CQDs, colloidal quantum dots; PCE, power conversion efficiency; PV, photovoltaic; DFT, density functional theory; VASP, Vienna Ab Initio Simulation Package; ^{1}H NMR, proton nuclear magnetic resonance; DMF, *N*,*N*-dimethylformamide; XPS, X-ray photoelectron spectroscopy; FET, field-effect transistor; FF, fill factor; EQE, external quantum efficiency

■ REFERENCES

(1) Konstantatos, G.; Howard, I.; Fischer, A.; Hoogland, S.; Clifford, J.; Klem, E.; Levina, L.; Sargent, E. H. Ultrasensitive Solution-Cast Quantum Dot Photodetectors. *Nature* **2006**, *442*, 180−183.

(2) Lee, J.-S.; Kovalenko, M. V.; Huang, J.; Chung, D. S.; Talapin, D. V. Band-Like Transport, High Electron Mobility and High Photoconductivity in All-Inorganic Nanocrystal Arrays. *Nat. Nanotechnol.* **2011**, *6*, 348−352.

(3) Sun, Q.; Wang, A.; Li, L. S.; Wang, D.; Zhu, T.; Xu, J.; Yang, C.; Li, Y. Bright, Multicoloured Light-Emitting Diodes Based on Quantum Dots. *Nat. Photonics* **2007**, *1*, 717−722.

(4) Fan, F.; Voznyy, O.; Sabatini, R. P.; Bicanic, K. T.; Adachi, M. M.; McBride, J. R.; Reid, K. R.; Park, Y.-S.; Li, X.; Jain, A.; Quintero-Bermudez, R.; Saravanapavanantham, M.; Liu, M.; Korkusinski, M.; Hawrylak, P.; Klimov, V. I.; Rosenthal, S. J.; Hoogland, S.; Sargent, E. H. Continuous-Wave Lasing in Colloidal Quantum Dot Solids Enabled by Facet-Selective Epitaxy. *Nature* **2017**, *544*, 75−79.

(5) Ip, A. H.; Thon, S. M.; Hoogland, S.; Voznyy, O.; Zhitomirsky, D.; Debnath, R.; Levina, L.; Rollny, L. R.; Carey, G. H.; Fischer, A.; Kemp, K. W.; Kramer, I.; Ning, Z.; Labelle, A. J.; Chou, K. W.; Amassian, A.; Sargent, E. H. Hybrid Passivated Colloidal Quantum Dot Solids. *Nat. Nanotechnol.* **2012**, *7*, 577−582.

(6) Liu, M.; Voznyy, O.; Sabatini, R.; García de Arquer, F. P.; Munir, R.; Balawi, A. H.; Lan, X.; Fan, F.; Walters, G.; Kirmani, A. R.; Hoogland, S.; Laquai, F.; Amassian, A.; Sargent, E. H. Hybrid Organic-Inorganic Inks Flatten the Energy Landscape in Colloidal Quantum Dot Solids. *Nat. Mater.* **2017**, *16*, 258−263.

(7) Chuang, C.-H. M.; Brown, P. R.; Bulović, V.; Bawendi, M. G. Improved Performance and Stability in Quantum Dot Solar Cells through Band Alignment Engineering. *Nat. Mater.* **2014**, *13*, 796−801.

(8) Lan, X.; Voznyy, O.; Kiani, A.; García de Arquer, F. P.; Abbas, A. S.; Kim, G.; Liu, M.; Yang, Z.; Walters, G.; Xu, J.; Yuan, M.; Ning, Z.; Fan, F.; Kanjanaboos, P.; Kramer, I.; Zhitomirsky, D.; Lee, P.; Perelgut, A.; Hoogland, S.; Sargent, E. H. Passivation Using Molecular Halides Increases Quantum Dot Solar Cell Performance. *Adv. Mater.* **2016**, *28*, 299−304.

(9) Xu, J.; Voznyy, O.; Liu, M.; Kirmani, A. R.; Walters, G.; Munir, R.; Abdelsamie, M.; Proppe, A. H.; Sarkar, A.; García de Arquer, F. P.; Wei, M.; Sun, B.; Liu, M.; Ouellette, O.; Quintero-Bermudez, R.; Li, J.; Fan, J.; Quan, L.; Todorovic, P.; Tan, H.; Hoogland, S.; Kelley, S. O.; Stefik, M.; Amassian, A.; Sargent, E. H. 2D Matrix Engineering for Homogeneous Quantum Dot Coupling in Photovoltaic Solids. *Nat. Nanotechnol.* **2018**, *13*, 456−462.

(10) McDonald, S. A.; Konstantatos, G.; Zhang, S.; Cyr, P. W.; Klem, E. J. D.; Levina, L.; Sargent, E. H. Solution-Processed PbS Quantum Dot Infrared Photodetectors and Photovoltaics. *Nat. Mater.* **2005**, *4*, 138−142.

(11) Luther, J. M.; Law, M.; Beard, M. C.; Song, Q.; Reese, M. O.; Ellingson, R. J.; Nozik, A. J. Schottky Solar Cells Based on Colloidal Nanocrystal Films. *Nano Lett.* **2008**, *8*, 3488−3492.

(12) Wang, X.; Koleilat, G. I.; Tang, J.; Liu, H.; Kramer, I. J.; Debnath, R.; Brzozowski, L.; Barkhouse, D. A. R.; Levina, L.; Hoogland, S.; Sargent, E. H. Tandem Colloidal Quantum Dot Solar Cells Employing a Graded Recombination Layer. *Nat. Photonics* **2011**, *5*, 480−484.

(13) Ip, A. H.; Kiani, A.; Kramer, I. J.; Voznyy, O.; Movahed, H. F.; Levina, L.; Adachi, M. M.; Hoogland, S.; Sargent, E. H. Infrared Colloidal Quantum Dot Photovoltaics *via* Coupling Enhancement and Agglomeration Suppression. *ACS Nano* **2015**, *9*, 8833.

(14) Baek, S.-W.; Ouellette, O.; Jo, J. W.; Choi, J.; Seo, K.-W.; Kim, J.; Sun, B.; Lee, S.-H.; Choi, M.-J.; Nam, D.-H.; Quan, L. N.; Kang, J.; Hoogland, S.; García de Arquer, F. P.; Lee, J.-Y.; Sargent, E. H. Infrared Cavity-Enhanced Colloidal Quantum Dot Photovoltaics Employing Asymmetric Multilayer Electrodes. *ACS Energy Lett.* **2018**, *3*, 2908−2913.

(15) Sun, B.; Ouellette, O.; García de Arquer, F. P.; Voznyy, O.; Kim, Y.; Wei, M.; Proppe, A. H.; Saidaminov, M. I.; Xu, J.; Liu, M.; Li, P.; Fan, J. Z.; Jo, J. W.; Tan, H.; Tan, F.; Hoogland, S.; Lu, Z. H.; Kelley, S. O.; Sargent, E. H. Multibandgap Quantum Dot Ensembles for Solar-Matched Infrared Energy Harvesting. *Nat. Commun.* **2018**, *9*, 4003.

DOI: 10.1021/acsenergylett.9b00388
ACS Energy Lett. 2019, 4, 1225−1230

(16) Jean, J.; Brown, P. R.; Jaffe, R. L.; Buonassisi, T.; Bulović, V. Pathways for Solar Photovoltaics. *Energy Environ. Sci.* **2015**, *8*, 1200−1219.
(17) Chapin, D. M.; Fuller, C.; Pearson, G. A New Silicon p-n Junction Photocell for Converting Solar Radiation into Electrical Power. *J. Appl. Phys.* **1954**, *25*, 676−677.
(18) Jo, J. W.; Choi, J.; García de Arquer, F. P.; Seifitokaldani, A.; Sun, B.; Kim, Y.; Ahn, H.; Fan, J.; Quintero-Bermudez, R.; Kim, J.; Choi, M.; Baek, S.-W.; Proppe, A. H.; Walters, G.; Nam, D.-H.; Kelley, S.; Hoogland, S.; Voznyy, O.; Sargent, E. H. Acid-Assisted Ligand Exchange Enhances Coupling in Colloidal Quantum Dot Solids. *Nano Lett.* **2018**, *18*, 4417−4423.
(19) Choi, H.; Ko, J.-H.; Kim, Y.-H.; Jeong, S. Steric-Hindrance-Driven Shape Transition in PbS Quantum Dots: Understanding Size-Dependent Stability. *J. Am. Chem. Soc.* **2013**, *135*, 5278.
(20) Zarghami, M. H.; Liu, Y.; Gibbs, M.; Gebremichael, E.; Webster, C.; Law, M. The Role of Intercalated Water in Multilayered Graphene Oxide. *ACS Nano* **2010**, *4*, 2475−2485.
(21) Rosson, T. E.; Claiborne, S. M.; McBride, J. R.; Stratton, B. S.; Rosenthal, S. J. Bright White Light Emission from Ultrasmall Cadmium Selenide Nanocrystals. *J. Am. Chem. Soc.* **2012**, *134*, 8006−8009.
(22) Kresse, G.; Hafner, J. Ab Initio Molecular Dynamics for Liquid Metals. *Phys. Rev. B: Condens. Matter Mater. Phys.* **1993**, *47*, 558−561.
(23) Kresse, G.; Furthmüller, J. Efficiency of Ab-Initio Total Energy Calculations for Metals and Semiconductors Using a Plane-Wave Basis Set. *Comput. Mater. Sci.* **1996**, *6*, 15−50.
(24) Keitel, R. C.; Weidman, M. C.; Tisdale, W. A. Near-Infrared Photoluminescence and Thermal Stability of PbS Nanocrystals at Elevated Temperatures. *J. Phys. Chem. C* **2016**, *120*, 20341−20349.
(25) Zherebetskyy, D.; Scheele, M.; Zhang, Y.; Bronstein, N.; Thompson, C.; Britt, D.; Salmeron, M.; Alivisatos, P.; Wang, L. W. Hydroxylation of the Surface of PbS Nanocrystals Passivated with Oleic Acid. *Science* **2014**, *344*, 1380−1384.
(26) Boles, M. A.; Ling, D.; Hyeon, T.; Talapin, D. V. The Surface Science of Nanocrystals. *Nat. Mater.* **2016**, *15*, 141−153.
(27) Morris-Cohen, A. J.; Malicki, M.; Peterson, M. D.; Slavin, J. W. J.; Weiss, E. A. Chemical, Structural, and Quantitative Analysis of the Ligand Shells of Colloidal Quantum Dots. *Chem. Mater.* **2013**, *25*, 1155−1165.
(28) Anderson, N. C.; Owen, J. S. Soluble, Chloride-Terminated CdSe Nanocrystals: Ligand Exchange Monitored by ^{1}H and ^{31}P NMR Spectroscopy. *Chem. Mater.* **2013**, *25*, 69−76.
(29) Reinhart, C. C.; Johansson, E. Colloidally Prepared 3-Mercaptopropionic Acid Capped Lead Sulfide Quantum Dots. *Chem. Mater.* **2015**, *27*, 7313−7320.
(30) Kuno, M.; Lee, J. K.; Dabbousi, B. O.; Mikulec, F. V.; Bawendi, M. G. The Band Edge Luminescence of Surface Modified CdSe Nanocrystallites: Probing the Luminescing State. *J. Chem. Phys.* **1997**, *106*, 9869−9882.
(31) Pal, D.; Stoleru, V. G.; Towe, E.; Firsov, D. Quantum Dot-Size Variation and Its Impact on Emission and Absorption Characteristics: An Experimental and Theoretical Modeling Investigation. *Jpn. J. Appl. Phys.* **2002**, *41*, 482−489.
(32) Voznyy, O.; Levina, L.; Fan, F.; Walters, G.; Fan, J. Z.; Kiani, A.; Ip, A. H.; Thon, S. M.; Proppe, A. H.; Liu, M.; Sargent, E. H. Origins of Stokes Shift in PbS Nanocrystals. *Nano Lett.* **2017**, *17*, 7191−7195.
(33) Choi, J. J.; Luria, J.; Hyun, B.-R.; Bartnik, A. C.; Sun, L.; Lim, Y.- F.; Marohn, J. A.; Wise, F. W.; Hanrath, T. Photogenerated Exciton Dissociation in Highly Coupled Lead Salt Nanocrystal Assemblies. *Nano Lett.* **2010**, *10*, 1805−1811.
(34) Sun, B.; Voznyy, O.; Tan, H.; Stadler, P.; Liu, M.; Walters, G.; Proppe, A. H.; Liu, M.; Fan, F.; Zhuang, T.; Li, J.; Wei, M.; Xu, J.; Kim, Y.; Hoogland, S.; Sargent, E. H. Pseudohalide-Exchanged Quantum Dot Solids Achieve Record Quantum Efficiency in Infrared Photovoltaics. *Adv. Mater.* **2017**, *29*, 1700749.
(35) Hossain Chowdhury, M. D.; Migliorato, P.; Jang, J. Low Temperature Characteristics in Amorphous Indium-Gallium-Zinc-Oxide Thin-Film Transistors Down to 10-K. *Appl. Phys. Lett.* **2013**, *103*, 152103.
(36) Rolland, A.; Richard, J.; Kleider, J. P.; Mencaraglia, D. Electrical Properties of Amorphous Silicon Transistors and MIS-Devices: Comparative Study of Top Nitride and Bottom Nitride Configurations. *J. Electrochem. Soc.* **1993**, *140*, 3679.
(37) Zhitomirsky, D.; Voznyy, O.; Levina, L.; Hoogland, S.; Kemp, K. W.; Ip, A. H.; Thon, S. M.; Sargent, E. H. Engineering Colloidal Quantum Dot Solids Within and Beyond the Mobility-Invariant Regime. *Nat. Commun.* **2014**, *5*, 3803.

DOI: 10.1021/acsenergylett.9b00388
ACS Energy Lett. 2019, 4, 1225−1230